Influence of Poloxamer on the Dissolution and Stability of Hot-Melt Extrusion–Based Amorphous Solid Dispersions Using Design of Experiments

Ashay Shukla[1] · Nagi Reddy Dumpa[1] · Rishi Thakkar[1] · Abhishek Shettar[1] · Eman Ashour[1] · Suresh Bandari[1] · Michael A. Repka[1,2]

Abstract

The current study aimed to see the effects of poloxamer P407 on the dissolution performance of hydroxypropyl methylcellulose acetate succinate (AquaSolve™ HPMC-AS HG)-based amorphous solid dispersions (ASD). A weakly acidic, poorly water-soluble active pharmaceutical ingredient (API), mefenamic acid (MA), was selected as a model drug. Thermal investigations, including thermogravimetry (TG) and differential scanning calorimetry (DSC), were conducted for raw materials and physical mixtures as a part of the pre-formulation studies and later to characterize the extruded filaments. The API was blended with the polymers using a twin shell V-blender for 10 min and then extruded using an 11-mm twin-screw co-rotating extruder. Scanning electron microscopy (SEM) was used to study the morphology of the extruded filaments. Furthermore, Fourier-transform infrared spectroscopy (FT-IR) was performed to check the intermolecular interactions of the components. Finally, to assess the *in vitro* drug release of the ASDs, dissolution testing was conducted in phosphate buffer (0.1 M, pH 7.4) and hydrochloric acid–potassium chloride (HCl-KCl) buffer (0.1 M, pH 1.2). The DSC studies confirmed the formation of the ASDs, and the drug content of the extruded filaments was observed to be within an acceptable range. Furthermore, the study concluded that the formulations containing poloxamer P407 exhibited a significant increase in dissolution performance compared to the filaments with only HPMC-AS HG (at pH 7.4). In addition, the optimized formulation, F3, was stable for over 3 months when exposed to accelerated stability studies.

Keywords amorphous solid dispersions · design of experiments · hot-melt extrusion · HPMC-AS · mefenamic acid · poloxamer P407

Introduction

In recent times, enhancing drug solubility has been an active area of research. Techniques including solid dispersions [1–3], inclusion complexes [4, 5], ultra-rapid freezing processes [6], melt sono-crystallization [7], nanocrystallization by anti-solvent addition [8], melt granulation techniques [9], and micronization by supercritical solvent are being used extensively. Among these approaches, hot-melt extrusion (HME), a solvent-free, continuous process, has observed various advantages [10–13]. The method of extrusion involves physically mixing the API with polymeric carriers and other excipients, which are then pumped through a barrel at elevated temperature and pressure to get the extruded products, usually in the form of filaments or granules [11, 14, 15]. The unstable materials at higher temperatures may cause the process to malfunction and the product to degrade [9, 16, 17]. Upon adding specific carriers and plasticizers, the thermal stability of an API can be improved to a great extent, promoting better extrusion processability while decreasing processing temperatures [18].

✉ Michael A. Repka
  marepka@olemiss.edu

1 Department of Pharmaceutics and Drug Delivery,
   School of Pharmacy, The University of Mississippi,
   University 38677, Mississippi, USA

2 Pii Center for Pharmaceutical Technology, The University
   of Mississippi, University 38677, Mississippi, USA

One such additive to improve the HME process is poloxamer P407. It is a water-soluble, non-ionic triblock copolymer made up of a hydrophobic residue of polyoxypropylene (POP) between the two hydrophilic units of polyoxyethylene (POE) [19, 20]. Poloxamer P407 has been previously used as a solubility or a dissolution enhancer due to its surface-active properties, low melting point, and bio-compatibility [21]. The solubility of many hydrophobic drugs can be improved by introducing a hydrophilic carrier into the formulation matrix, and these might include polyvinylpyrrolidone (PVP) [22], hydroxypropyl methylcellulose (HPMC) [23], or Eudragit® [24]. Although these polymers' solubilization capacity might be limited, their supersaturation may lead to recrystallization of the API [25]. Since HPMC AS HG solubilizes at a pH above 7, it presented a perfect environment to hinder the drug release in acidic media. Some of the options that were considered to be used to enhance the solubility of the HPMC AS-MA mix were Gelucire 50/13, poloxamer p188, and poloxamer P407. Experiments were performed to generate formulations with Gelucire 50/13 at different concentrations, and observations were made. Literature suggests that poloxamer P407 has been more efficient, specifically when the poloxamer concentration in a formulation is above 10%. This is because of the higher hydrophobicity and lower critical micellar concentration than P188. The effect of poloxamer P407 in preventing recrystallization due to supersaturation of the polymer is investigated in this research study using HPMC-AS HG as a carrier. Furthermore, P407 also acts as a solubility or dissolution enhancer which has a low melting point, surfactant properties and is orally safe to be used [26–29].

In this study, the impact of different concentrations of poloxamer P407 on the dissolution performance of HPMC-AS HG-mefenamic acid-based ASDs was evaluated. Using the design of experiments (DoE), different formulations containing 20–40% w/w MA, 40–80% w/w HPMC-AS HG, and 0–20% w/w poloxamer P407 were prepared. These ASDs were exposed to thermal, morphological, and performance testing. The addition of poloxamer P407 to the formulation was observed to significantly influence the performance of the extruded filaments under discussion at pH 7.4. An added importance of an improved release of a weakly acidic and poorly soluble drug, such as MA (solubility: 20 mg/L, pKa: 4.2 and logP: 5.12), at a higher pH is the circumvention of its gastrointestinal side effects, such as bleeding and ulceration [25].

Materials and Methods

Materials

Mefenamic acid was purchased from TCI America (Portland, OR, USA). AquaSolve™ HPMC-AS HG was received as a gift from Ashland (Wilmington, DE, USA). Kolliphor P407 was received as a gift from BASF SE (Ludwigshafen, Germany). Sodium hydroxide and potassium phosphate were purchased from Acros Organics (NJ, USA). All other chemicals, solvents, and reagents used in this study were of analytical grade and obtained from Fisher Scientific (Fair Lawn, NJ, USA).

TGA

TGA (Perkin Elmer, Pyris 1, Shelton, CT, USA) was used to ascertain the thermal degradation temperature of MA and other components of the formulations [30]. TGA was performed in the heating range of 25–300°C at an accelerated rate of 10°C/min. A nitrogen purge was set at 20 mL/min, and approximately 10 mg of each sample was weighed in the platinum pan and analyzed using the Pyris 1 software.

Designing the Formulations

Design of experiments (DoE) is an essential tool used in statistical analysis. It plays a vital role in applying the quality by design (QbD) approach in industrial and laboratory-based research setting [31]. It has been observed that ever since ICH Q8 Guidelines highlighted the use of DoE approaches in the scientific and industrial domains, there has been a significant rise in the utilization of DoE [32, 33]. Furthermore, the availability of various statistical and designing software at scientists' disposal increased the opportunities to exploit this approach at a much greater pace [34]. The software used in this study was Design Expert 11. The design selection was based on the prediction-based optimality criteria [35], and the applied approach depended on the drug dissolution studies, taking into account the crystallinity of the formulations observed via differential scanning calorimetry. The "mixture" DoE methodology was selected, staying as close as possible to the abovementioned responses. Within the mixture DoE methodology, to minimize the average prediction variance over the experimental region, the I optimal criterion was utilized [36].

Following the I optimality criterion, if P1 is considered to be the average prediction of the variance of Design 1 and P2 is considered to be the average prediction of the variance of Design 2, then I-efficiency of Design 1 can be stated as; P2/P1 and vice versa for Design 2. If the value of I-efficiency for Design 1 is more significant than 1, it depicts that Design 1 is better than Design 2 regarding average prediction variance. When D-optimal designs were compared with I-optimal designs, it was found that in the case of D-optimal designs, the median variance of prediction is about 50% larger than that of I-optimal designs. Furthermore, it was observed that the I-efficiency of I-optimal designs was higher (1.00) than D-optimal designs, which confirmed the effectiveness of the

I-optimal mixture design for this study [35–37]. The three components of the design were A-HPMC-AS HG, B-MA, and C-Kolliphor P407. Each component's lower and upper limits were set so that the mixture components of each run would add up to 100. The target profile of the optimized formulation is described in Table I.

After the formulations were obtained, the response was added to the design. Since the crystallinity of the formulations was not quantified, only one response could be used to optimize the formulations, i.e., drug release (%). Further optimization was based on the solid-state characterization of these formulations. The processing parameters used while performing extrusion were based on the results of the screening studies described in the previous section.

Hot-Melt Extrusion

After going through the preliminary formulation data, processing parameters for HME were finalized, and the extrusion process was carried out. The composition of different formulations is listed in Table II. Physical mixtures of formulations were prepared by weighing the exact amount of the drug and the polymers according to the formulation design and blending them using a V-blender (Globe Pharma Maxiblend™, New Brunswick, NJ, USA). These blended mixtures were then processed using HME. A screw speed of 50 rpm with an optimized screw configuration consisting of three mixing zones was used for extrusion [38]. A 2.5-mm die was used, and different temperatures for different formulations were set, as mentioned in Table II. The feed rate was set at 4% (approximately 1.5 g/min), processing temperatures were between 140 and 160°C, and torque was carefully observed throughout the process. The extruded filament obtained was milled using a laboratory grinder and sieved through ASTM #30 mesh. The sieved powder was stored in sealed glass vials preserved in a desiccator until further analysis.

Table I Target Profile

Element/attribute	Target	QTPP	CQA
Route of administration	Oral	✓	
Dosage form	Capsule	✓	
Assay	90–110%	✓	✓
Content uniformity	USP < 905 >	✓	✓
Strength	100 mg	✓	
Stability	3 months accelerated stability	✓	
Dissolution	100% (2 h)	✓	✓
Solid state	Amorphous	✓	✓
Compatibility	Excipients	✓	✓

QTPP quality target product profile, *CQA* critical quality attribute

Table II Details of Formulations

Formulation	% Mefenamic acid	% Aquasolve HPMC-AS HG	% Kolliphor P407
F1	20	80	0
F2	20	70	10
F3	20	60	20
F4	30	70	0
F5	30	60	10
F6	30	50	20
F7	35	50	15
F8	40	60	0
F9	40	55	5
F10	40	50	10
F11	40	40	20

DSC

DSC (TA Instruments Discovery Series DSC 25, New Castle, DE, USA) analysis was conducted to analyze the glass transition temperature and the melting point of pure ingredients and different formulations [39, 40]. The analysis was performed over the temperature range of 25 to 300°C at the heating rate of 10°C/min, and the nitrogen purge was set at 20°C/min. Samples (5–15 mg) were weighed in an aluminum pan and sealed with a hermetic lid. The TRIOS software was used to analyze the solid-state characteristics and thermal stability of the pure drug, polymers, and formulations.

FT-IR

An Agilent Technologies Cary 600 Series FTIR Spectrophotometer (Santa Clara, CA, USA) was used to study the interaction between the drug and the polymeric carrier. Samples of pure drugs, polymers, and formulations were scanned over a frequency range of 4000–400 cm^{-1}. The data was collected and analyzed using the Resolutions Pro software.

SEM

SEM study was performed to evaluate the surface morphology of the pure drug and formulations using JEOL JSM 5600 SEM (JEOL, Peabody, MA, USA) at an accelerated voltage of 5 kV [41]. Hummer sputtering system (Anatech Ltd., Springfield, VA, USA) was used to prepare the sample in a high vacuum evaporator. Carbon pads were mounted on an aluminum base, and the extrudates were powdered and placed on these adhesive pads. This step was followed by sputter coating with

gold. After the gold coating, these samples were put under the microscope, and the images were captured.

Drug Content

Milled extrudates equivalent to 50 mg of the pure drug were weighed and transferred into 50 mL volumetric flasks, to which 40 mL methanol was added. The volumetric flask was sonicated for 20 min using a Branson 2800 Ultrasonic Bath (Cleanosonic, Richmond, VA, USA) to solubilize the drug entirely in the solvent. Once the drug was solubilized, volume was made up to the 50-mL mark using methanol. This sample solution was diluted appropriately and analyzed for MA content at a wavelength of 285 nm using a UV–Visible Spectrophotometer (Genesys 6; Thermo Scientific., USA).

Dissolution Studies

Hanson SR8 Plus Dissolution System (Chatsworth, CA) USP Type II (Paddle) Apparatus was used to conduct the *in vitro* dissolution studies. The milled filaments (100 mg MA equivalent) and the pure drug were weighed by the drug load equivalent to 100 mg MA, passed through sieve #30, and filled into hard gelatin capsules (standard "00" size). Dissolution studies were performed using hydrochloric acid–potassium chloride (HCl-KCl) buffer (0.1 M, pH 1.2) and phosphate buffer (0.1 M, pH 7.4) for 120 min. These capsules were placed in dissolution vessels filled with 900 mL buffer solution using sinkers. The water bath temperature was maintained at $37 \pm 0.5°C$, and the paddle speed was set at 50 RPM. Samples (3 mL) were withdrawn from the dissolution vessels at 15, 30, 45, 60, 90, and 120 min [42]. The samples were filtrated using a 10-μ Amicon filter. The samples were diluted 10 folds and analyzed using a UV–visible (UV–vis) spectrophotometer.

Stability Studies

The accelerated stability studies were conducted for 3 months for the optimized formulations (F3, F7, F9, F10) at $40°C \pm 2°C$ and $75\% \pm 5\%$ RH [43]. These were further characterized using DSC, drug content uniformity, and dissolution studies. All parameters used during these studies were kept the same as those with initial samples. The similarity factor (f2) and dissimilarity factor (f1) were calculated using the formulae provided her e[44–46].

$$f_2 = 50\log\left\{\left[1 + \frac{1}{n}\sum_{n-1}^{n}\left[R_t - T_t\right]^2\right]^{-0.5} \times 100\right\} \quad (1)$$

$$f_1 = \left\{\frac{\left[\sum_{t=1}^{n}R_t - T_t\right]}{\sum_{t=1}^{n}R_t}\right\} \quad (2)$$

Results

TGA

TGA was performed to determine the thermal stability of MA and all the excipients used in HME processing. TGA analysis revealed that the thermal degradation temperature of MA was $238 \pm 2°C$, which aligns with the previous literature discussing the degradation of MA [47]. In addition, both HPMC-AS HG and Kolliphor P407 were stable over 300°C. Therefore, the processing temperature was set less than the degradation temperature of MA, HPMC-AS HG, and Kolliphor P407 to prevent any degradation during the extrusion process.

### Differential Scanning Calorimetry

The DSC thermogram depicted two endothermic peaks of MA at 174°C and 231°C, observed because MA exists in two polymorphic forms. The first endothermic peak is the conversion of MA form 1 to its metastable state, MA form 2, whereas the second endothermic peak corresponds to the melting temperature of MA [48, 49]. MA was found to have converted entirely to its amorphous form in the manufactured solid dispersions (F1 through F6). However, the DSC thermograms of the extruded filaments having the higher drug load of MA retained trace crystallinity.

This can be seen from the low-intensity peaks of MA in Fig. 1. In formulations F7 through F11, the crystalline peak of MA reduced in intensity and was shifted to lower temperatures suggesting the partial conversion of MA into its amorphous form (Fig. 2). However, the MA crystals were dispersed in the polymeric matrix forming solid crystalline dispersions [50].

FT-IR

The FT-IR spectra of all the samples, shown in Fig. 3, were consistent with the IR spectrum of the pure MA [49]. The peaks at 1646, 1255, and 889 cm^{-1} represent N–H amine bending, aromatic amine stretch, and aromatic C$=$C bending, respectively. Further, the solid dispersions of MA and Kolliphor P407 observed no significant difference from the reference peak pure MA. However, it was detected that the polymer's ether (R-O-R) vibrations shifted from 2910 cm^{-1} to a lower wavenumber of 2860–2870 cm^{-1}.

Fig. 1 Representative DSC thermograms of pure components and formulations (F1–F6).
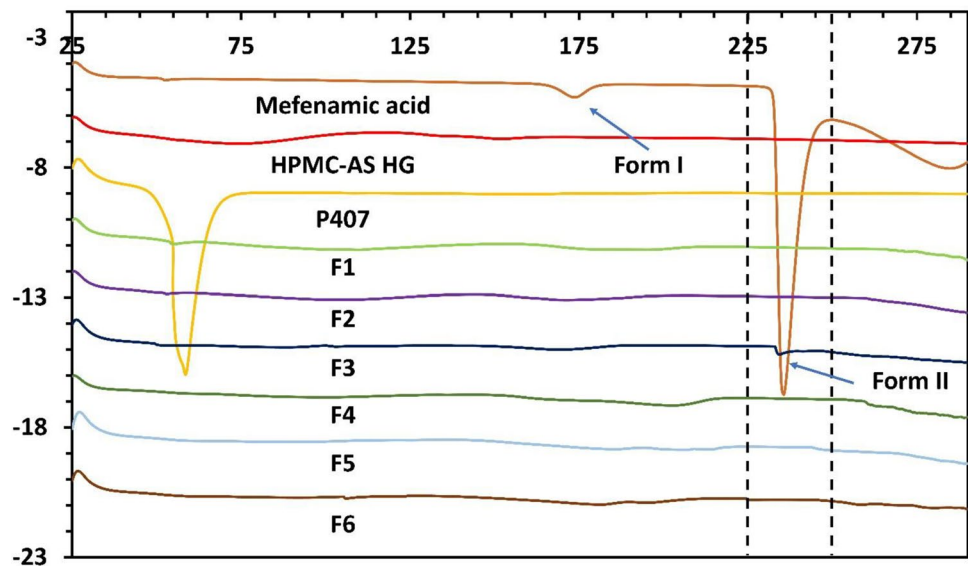
Fig. 2 Representative DSC thermograms of pure components and formulations (F7–F11).
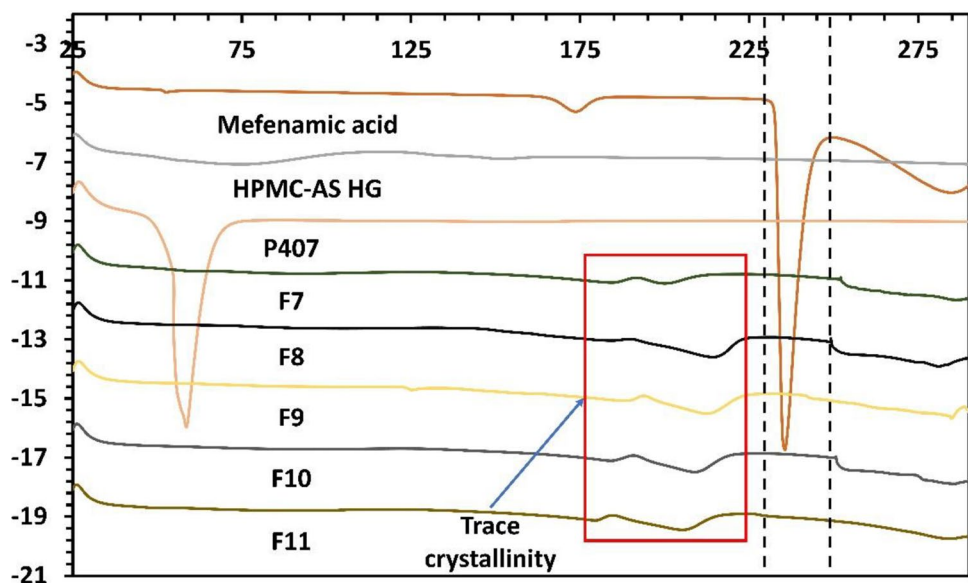
This resulted from the hydrogen bonding between the drug and the polymer [51].

SEM

The SEM images of the pure drug indicate that there are smaller crystalline particles accumulated on and around the enormous crystal in the case of pure MA. However, when the amorphous solid dispersions' SEM images were investigated, the smaller crystalline particles were utterly absent due to the drug's and the polymer's absolute mixture at a molecular level (Fig. 4). These observations can corroborate the DSC results discussed earlier in this manuscript.

Content Uniformity

The drug content uniformity of the formulations was analyzed, and the results were found to be within the acceptable range set by the United States Pharmacopoeia (USP), which is 90–110% for MA. The drug content ($n=3$) was 90.9 to 101% for all formulations. It can be seen from Table III that even at lower drug loads (F1, F2, F3), the HME process is capable of maintaining uniform drug content.

In Vitro Dissolution Studies

The *in vitro* release profiles of the formulations were studied, and it was observed that there was a significant improvement in the release of MA from the formulations which contained

Fig. 3 FTIR of pure mefenamic acid and the formulations, representing the compatibility and interactions between API and the polymers used.
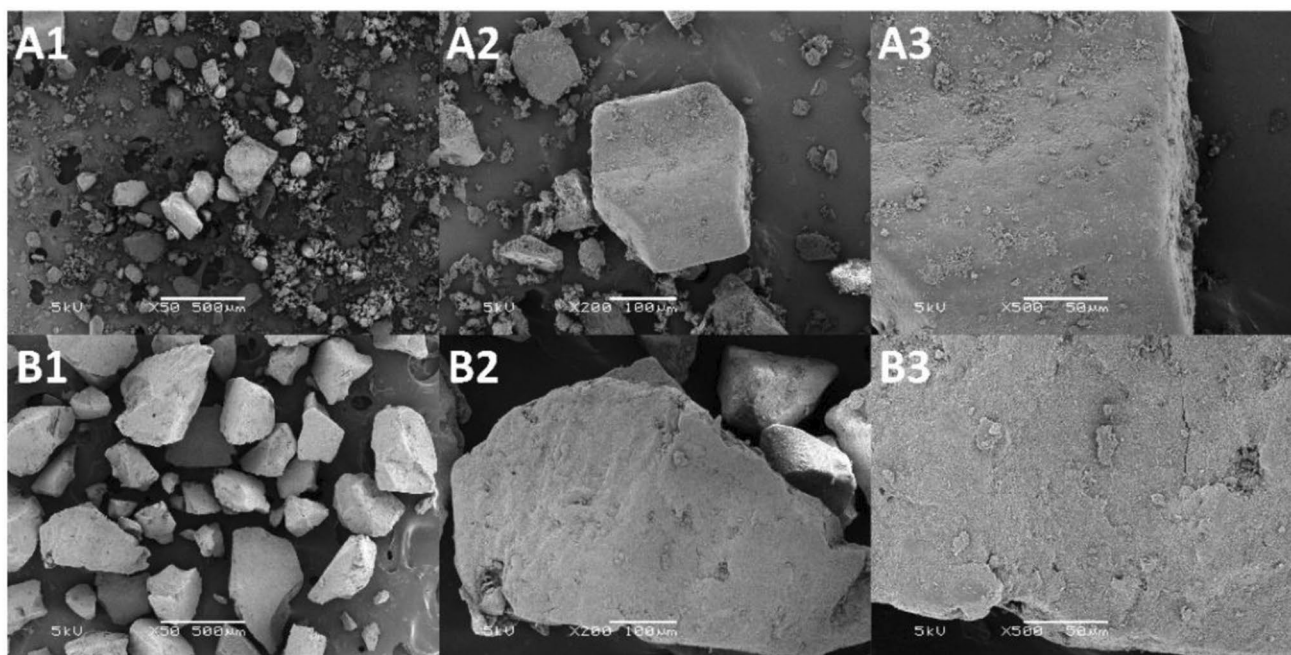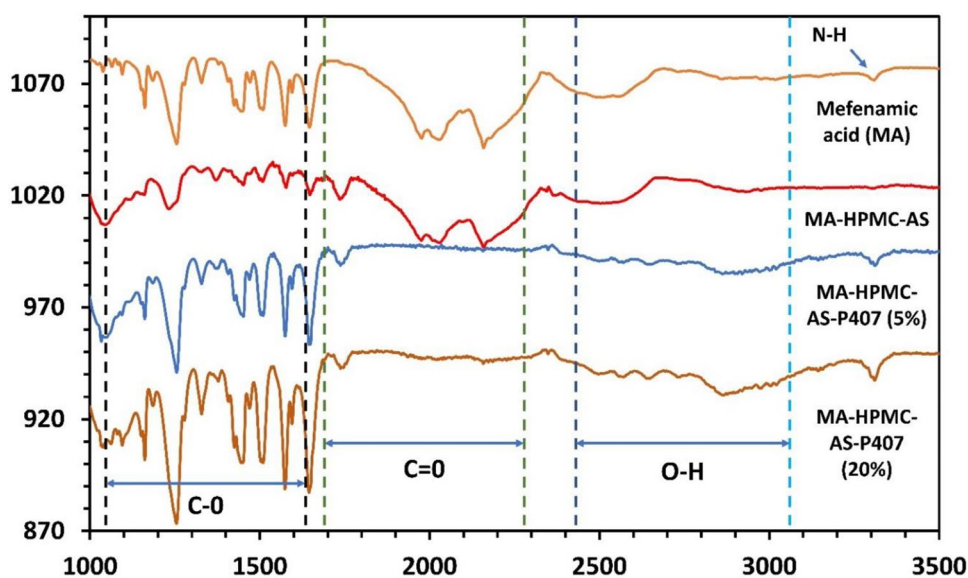
Fig. 4 SEM images of the drug (A1–A3) and selected optimized formulation (B1–B3) describe the pure API morphology and the solid dispersions in formulation F3.

poloxamer. It was also observed that there was a decline in the drug release of the formulations by increasing the drug load. A correlation was also observed between the amount of poloxamer and the drug release.

This behavior can be attributed to several physical processes occurring during the dissolution of the ASDs under discussion. Adding a hydrophilic additive such as poloxamer P407 can increase the wettability of the hydrophobic surfaces of MA-HPMC-AS HG solid dispersions, thereby facilitating accelerated drug release [52]. Moreover, the

hydrophilic carrier also reduces agglomeration and aggregation of the drug particles, facilitating their contact with the dissolution medium, which in turn enhances the dissolution rate and maintains the drug supersaturation [53]. This phenomenon could also prevent the recrystallization of the drug in the medium as poloxamer behaves as a polymeric surfactant and thereby could have stabilized the solubilized drug molecule [54]. HPMC-AS HG has a high ratio of acetyl:succinoyl substitutions. This chemistry of HPMC-AS HG is responsible for its pH-dependent solubility (more

Table III Drug Content

Formulation	(%) Drug content ($n = 3$)
F1	98.46 ± 3.2
F2	101.00 ± 2.7
F3	100.28 ± 3.6
F4	91.95 ± 4.2
F5	94.83 ± 3.4
F6	90.92 ± 2.2
F7	99.48 ± 3.8
F8	98.61 ± 1.4
F9	95.98 ± 1.2
F10	95.25 ± 4.8
F11	97.63 ± 4.6

significant than pH 6.8) [23]. This would prevent the release of MA in an acidic medium (i.e., the physiological pH of the stomach) and target it to the intestine. The main reason for the targeted release of MA in the intestine was to circumvent its GI side effects [55]. Being a non-selective Cyclooxygenase (Cox1 and Cox2) inhibitor, MA inhibits Cyclooxygenase 1 in the stomach, which participates in various pathways responsible for protecting the GI lining from the harsh acidic environment. This unwanted inhibition is the source of multiple GI side effects such as abdominal pain, constipation, diarrhea, and heartburn [56].

Figure 5 shows a correlation between the increase in drug release from the formulation and the increase in poloxamer concentration. For formulations F1, F2, and F3, where the drug load was set to 20%, an increase in poloxamer concentration was observed in an increase in drug release. This phenomenon can be explained by the mechanism mentioned above of poloxamer, which increases the dissolution rate and the solubilization of the drug in the medium due to its surfactant properties. Furthermore, this trend was also observed in the formulations F4, F5, and F6, where the drug load was set to 30%, and the amount of poloxamer varied from 0 to 20%. These observations for formulations F1 to F6 suggest that 20% of poloxamer can enhance the dissolution rate and the solubility (20-fold) of MA-HPMC-AS HG ASDs with up to 30% of drug load. For formulation F10 with 40% drug load and 10% poloxamer, a superior drug release profile was observed compared to F11 with 40% drug load and 20% poloxamer. This observation can be attributed to two main reasons. First, a higher concentration of surfactant (F11),
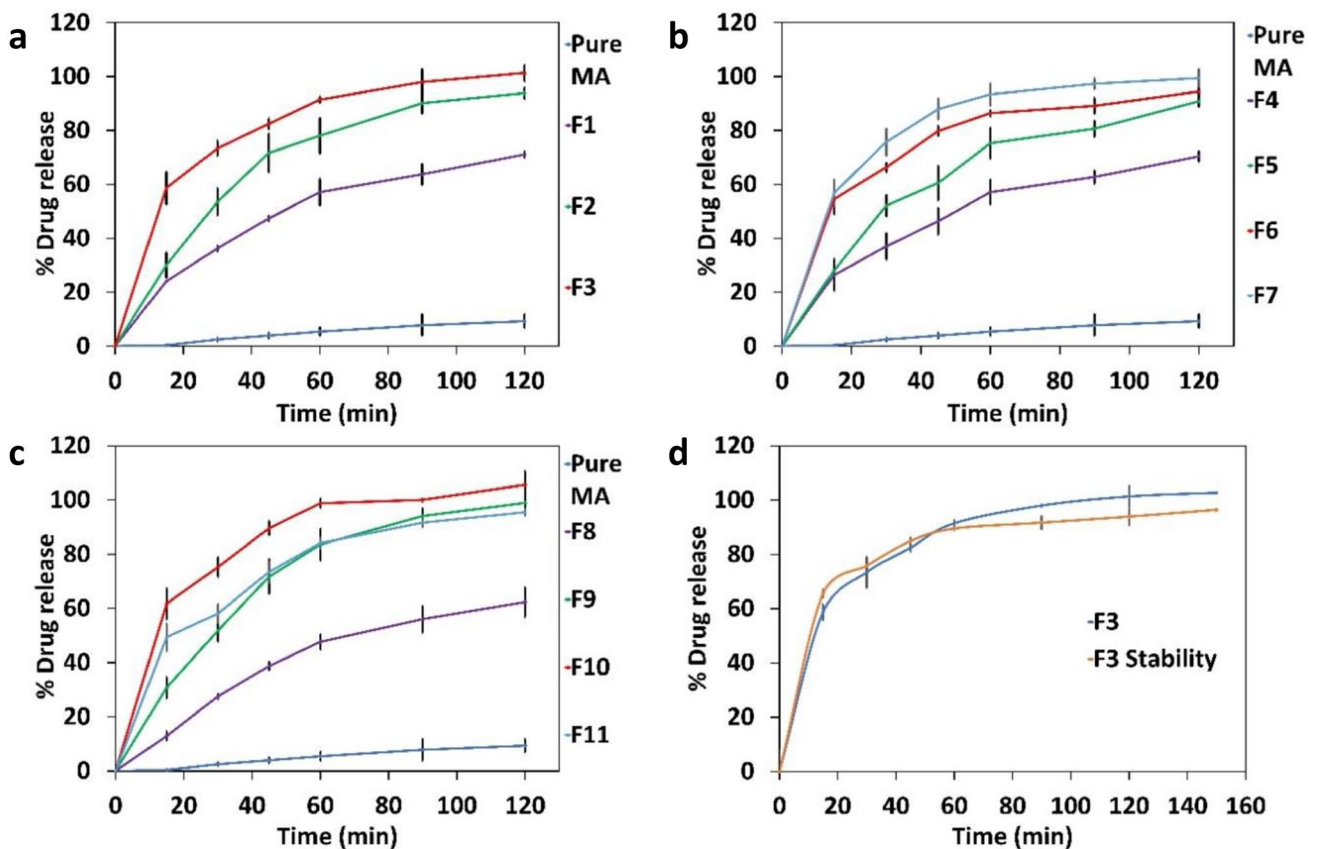
Fig. 5 Drug release profiles of **a** formulations F1–F3, **b** formulations F4–F7, **c** formulations F8–F11, and **d** optimized formulation F3, before and after stability study.

which if above critical micellar concentration (CMC), leads to the formation of bigger micelles with a lower surface area which hindered drug release as observed by Anderberg *et al.* [57]. Second, poloxamer has the capability of increasing the viscosity of the diffusion layer at a higher concentration. The increased viscosity of the diffusion layer due to the gel-forming capability of poloxamer in F11 may be responsible for the superior performance of F10. This same pattern can be observed with formulations F5, F6, and F7 because of the higher drug load and varying surfactant ratios [58]. Formulations F2 and F3 do not follow this trend because of a low drug load which is not affected by the hindering property of poloxamer 407.

When the dissolution studies were performed with selected formulations (pure MA, F3, F7, F10) using pH 1.2 simulated gastric fluid (enzyme free), less than 0.6% drug release was observed after 120 min. Therefore, it could be further stated that the site-specificity of the formulations was successfully achieved.

Regarding the extrusion parameters, the screening studies presented some valuable insights employed while deciding on the final parameters. For example, on increasing the extrusion temperature above 160°C, it was observed that the extrudates started losing their firmness and were further liquefied on increasing the temperature to 190°C. On the other hand, when the temperature was decreased below 140°C, the torque went beyond the permissible limit, and hence the extrusion was not performed below 140°C.

Statistical Interpretations and DoE Discussion

The model *F*-value from the design was 6.74, which implies that the model is significant. There is only a 1.89% chance that an *F*-value this large could occur due to noise. *P*-values less than 0.0500 indicated that the model terms are significant. A, B, and AC are significant model terms in this case. Values greater than 0.1000 indicate that the model terms are not significant. If there are many insignificant model terms (not counting those required to support hierarchy), the model reduction might improve this model.

Furthermore, a negative predicted R^2 implies that the overall mean may better predict the response than the current model. A higher-order model may also predict better precision measures in some cases, thereby giving a better signal-to-noise ratio. A ratio greater than 4 is desirable. Here, the ratio of 6.644 indicates an adequate signal (Table IV). Thereby, this model can be used to navigate the design space.

Furthermore, the coefficient estimate represents the expected change in response per unit change in factor value when all remaining factors are held constant. The intercept in an orthogonal design is the overall average response of all the runs. The coefficients are adjustments around that average based on the factor settings. When the factors are orthogonal, the VIFs are 1; VIFs greater than 1 indicate multi-collinearity, and the higher the VIF, the more severe the correlation of factors. As a rough rule, VIFs less than 10 are tolerable. These details for the current study are described in Table V.

When the predicted *versus* residual graph was analyzed, it was observed that all the formulations were linear, and the variability was uniform all along the axis. There was no curvature or outliers; hence, the assumptions of this model are believed to be accurate. Furthermore, the variance was constant with the mean throughout the graph, and the constant variance assumption was not violated. The regression graphs in Fig. 6 describe the relationship between the formulation's independent and dependent variables. As it can be very easily noticed from the actual *versus* predicted graph, there is a positive relationship between the independent and the dependent variables in the formulation. The response

Table V Fit Statistics

Std. dev	6.40	R^2	0.8490
Mean	92.96	Adjusted R^2	0.7231
C.V. %	6.89	Predicted R^2	0.0164
-	-	Adequate precision	6.6442

CV coefficient of variation

Table IV Analysis of Variance

Source	Sum of squares	df	Mean square	*F*-value	*p*-value	
Model	1381.91	5	276.38	6.74	0.0189	Significant
[(1)]Linear mixture	883.19	2	441.60	10.78	0.0103	
AB	37.34	1	37.34	0.9113	0.3766	
AC	491.12	1	491.12	11.99	0.0134	
BC	132.60	1	132.60	3.24	0.1221	
Residual	245.87	6	40.98	-	-	
Lack of fit	245.87	5	49.17	-	-	
Pure error	0.0000	1	0.0000	-	-	
Cor total	1627.78	11	-	-	-	

used in this prediction was % drug release, and with the help of regression analysis, it could be further confirmed that the formulations were significantly influenced by poloxamer 407. The formulations with 0% poloxamer 407 can be seen at the lower end of the graph, while the formulations with some amount of poloxamer 407 are at the top end (Table VI).

Figure 7 demonstrates that there could be 42 possible formulations within the limits of this design that could give a 100% drug release, and the optimized formulation can be selected from these 42 formulations. For example, formulation #34 could be selected as an optimized formulation because it resembles formulation F3. Furthermore, formulation F3 had the MA completely converted into an amorphous form, was compatible with the ingredients, and had acceptable drug content uniformity.

The thermogram obtained after DSC (Fig. 8) showed no recrystallization peak in the case of formulation F3, while there appears to be some recrystallization in formulations F7, F9, and F10. The drug content uniformity was assessed and found to be within the acceptable range by the USP (93.18–102.88%).

The optimized formulation was also evaluated for its drug release profile by performing dissolution studies, and the release profile can be seen in Fig. 5. The similarity factor (f2) and dissimilarity factor (f1) were calculated using the formulae. They were found to be well within the range of a stable formulation (f1 = 5.55–9.05, f2 = 56.66–64.89). Therefore, as far as the optimized formulation was concerned, only one could be considered an optimized formulation.

It could be observed from the release profiles, solid-state characterization, and stability studies that formulation F3 is the one which had a 100% drug release, had converted entirely into an amorphous form, and remained stable after 3 months of accelerated stability studies.
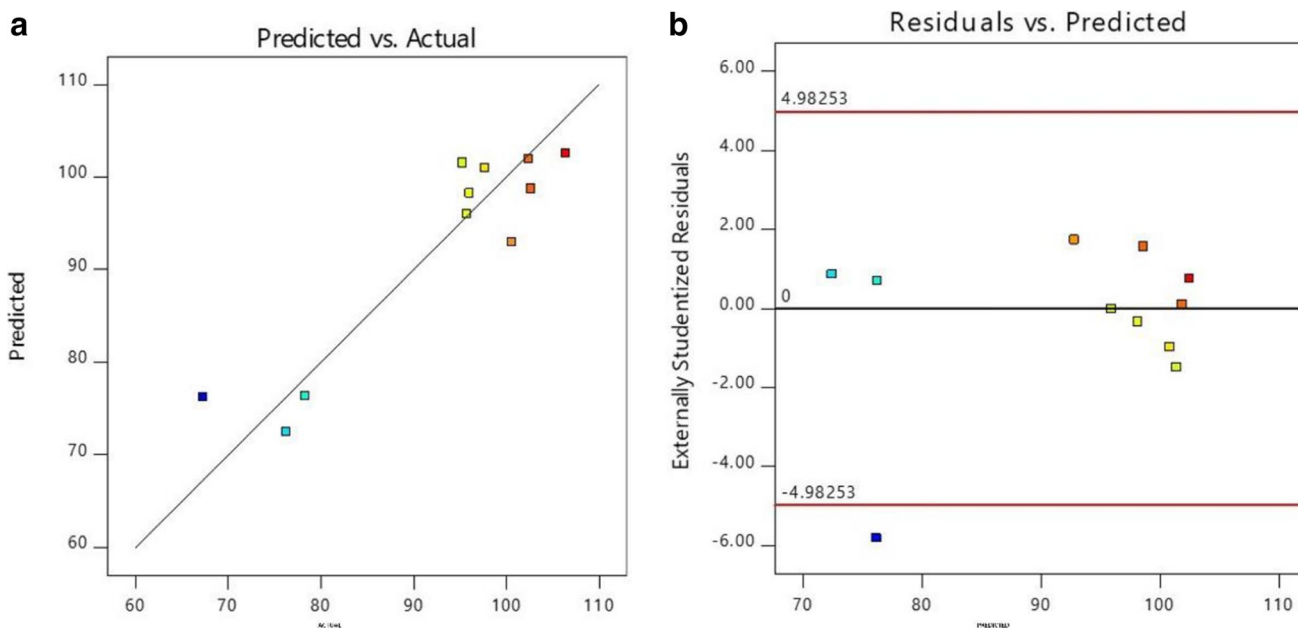

Fig. 6 **a** Predicted vs. actual graph represents the positive relationship between the dependent and the independent variables, and **b** residual vs. predicted graph represents the linearity and uniformity of the formulations with the model.

**Table VI** The Coefficient in Terms of Coded Factors

Component	Coefficient estimate	df	Standard error	95% CI low	95% CI high	VIF
A-HPMC AS-HG	76.28	1	5.67	62.42	90.15	2.71
B-Mefenamic acid	106.59	1	33.94	23.53	189.64	39.10
C-poloxamer P407	9.26	1	36.18	− 79.27	97.79	36.94
AB	− 60.91	1	63.80	− 217.03	95.21	19.11
AC	223.57	1	64.58	65.55	381.59	16.23
BC	171.81	1	95.51	− 61.90	405.51	27.88

CI confidence interval, *VIF* variance inflation factor

Desirability = 1.000
Solution 25 out of 42
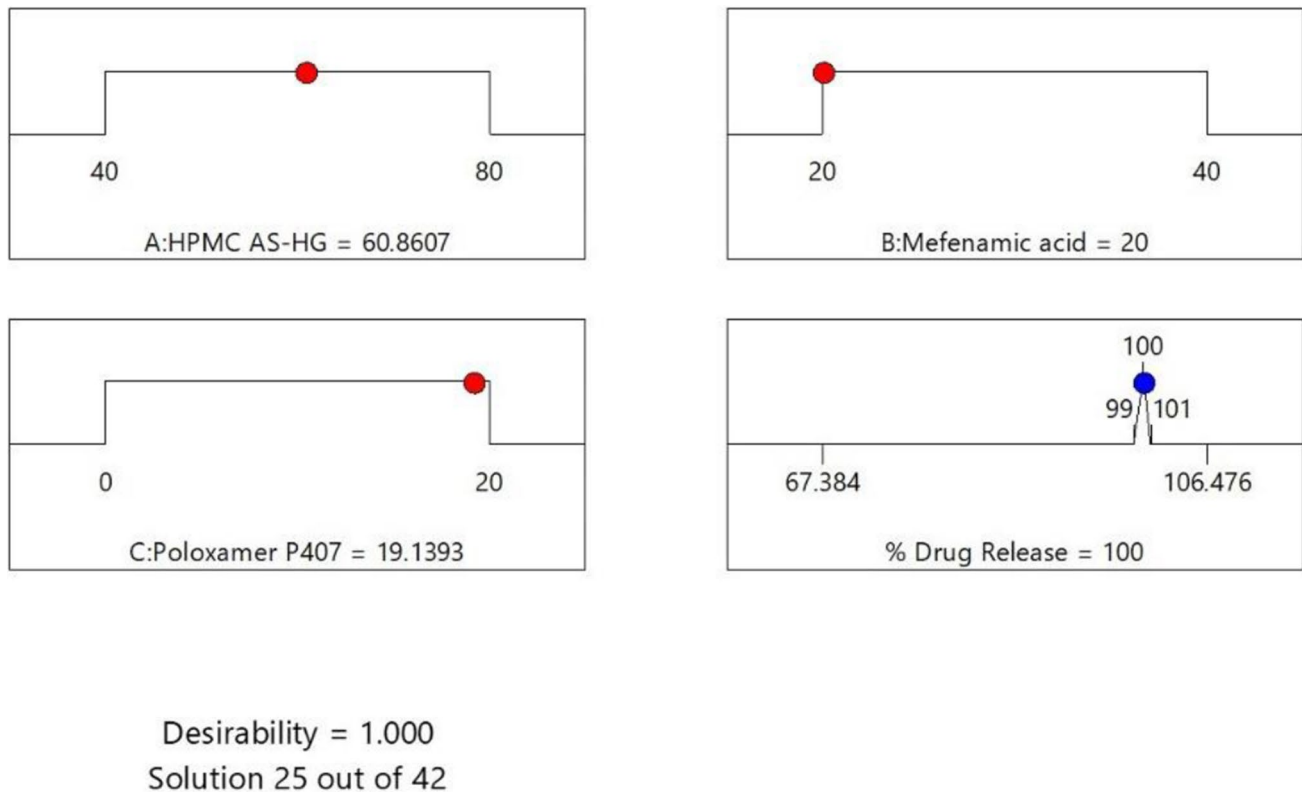
Fig. 7 Numerical optimization demonstrates the optimized formulation (F3) as one of the 42 numerically optimized formulations.

Fig. 8 DSC thermograms of the formulations after 3-month stability study at RH 75%±5% and temperature 40°C±2°C.
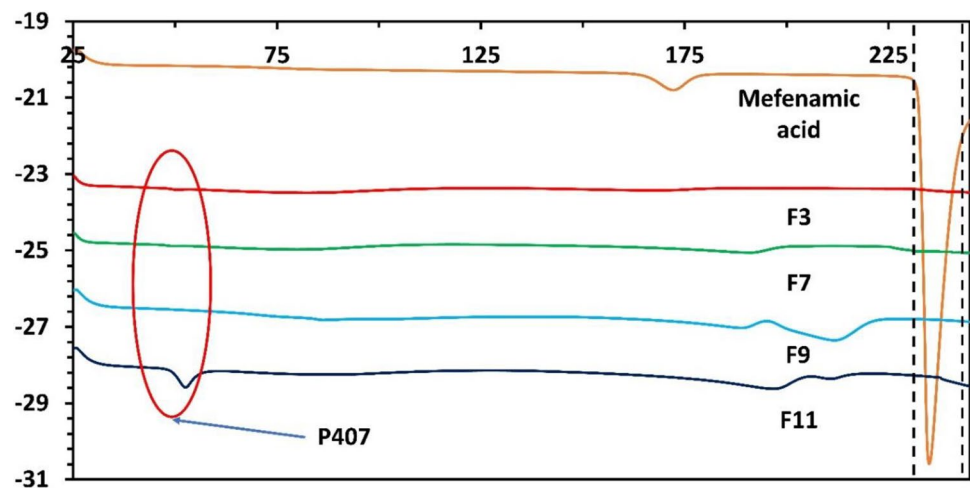
Conclusion

Solid dispersions of MA (20%, 30%, 35%, and 40% w/w) with varying ratios of AquaSolve™ HPMC-AS HG and Kolliphor® P407 (0%, 10%, and 20% w/w) were successfully prepared using hot-melt extrusion technology. The dissolution rate of mefenamic acid from HPMC-AS HG solid dispersions was observed to be better than the pure drug. Furthermore, the addition of Kolliphor® P407 enhanced the dissolution rate compared to pure MA. The enhanced solubilization can be attributed to the amorphous conversion of MA confirmed by solid-state characterization techniques, the enhanced wettability of the formulation due to the hydrophilicity of the additive, and finally, the surfactant property of the additive, which maintained the supersaturation of the drug in the dissolution media. The additive concentration depicted a strong correlation with the dissolution behavior. However, on increasing the

drug load above 20%, it was speculated that poloxamer started forming bigger micelles inhibiting the drug release after reaching critical micelle concentration (CMC). Stability studies showed that formulation F3 was stable after 3 months of accelerated stability study at RH $75\% \pm 5\%$ and temperature $40°C \pm 2°C$. Therefore, it was confirmed that F3 could be considered the optimized formulation. In conclusion, this study provides insights into the impact of surface-active, hydrophilic carriers on the dissolution behavior of ASD and further sheds light on their limitations in terms of drug loads and acceptable concentration ranges for preparing a stable formulation with notable solubility advantage.

Declarations

Conflict of Interest The authors declare no competing interests.

References

1. Crowley MM, et al. Pharmaceutical applications of hot-melt extrusion: part I. Drug Dev Ind Pharm. 2007;33:909–26.
2. Jermain SV, et al. In vitro and in vivo behaviors of KinetiSol and spray-dried amorphous solid dispersions of a weakly basic drug and ionic polymer†. Mol Pharm. 2020;17:2789–808.
3. Thakkar R, Thakkar R, Pillai A, Ashour EA, Repka MA. Systematic screening of pharmaceutical polymers for hot melt extrusion processing: a comprehensive review. Int J Pharm. 2020;576:118989.
4. Sherje AP, Jadhav M. β-Cyclodextrin-based inclusion complexes and nanocomposites of rivaroxaban for solubility enhancement. J Mater Sci Mater Med. 2018;29:186.
5. Mandati P, et al. Hot-melt extrusion–based fused deposition modeling 3D printing of atorvastatin calcium tablets: impact of shape and infill density on printability and performance. AAPS PharmSciTech. 2022;24:13.
6. Sahakijpijarn S, et al. Using thin film freezing to minimize excipients in inhalable tacrolimus dry powder formulations. Int J Pharm. 2020;586: 119490.
7. Manish M, Harshal J, Anant P. Melt sonocrystallization of ibuprofen: effect on crystal properties. Eur J Pharm Sci Off J Eur Fed Pharm Sci. 2005;25:41–8.
8. Bajaj A, Rao MRP, Pardeshi A, Sali D. Nanocrystallization by evaporative antisolvent technique for solubility and bioavailability enhancement of telmisartan. AAPS PharmSciTech. 2012;13:1331–40.
9. Kittikunakorn N, Sun CC, Zhang F. Effect of screw profile and processing conditions on physical transformation and chemical degradation of gabapentin during twin-screw melt granulation. Eur J Pharm Sci Off J Eur Fed Pharm Sci. 2019;131:243–53.
10. Repka MA, et al. Pharmaceutical applications of hot-melt extrusion: Part II. Drug Dev Ind Pharm. 2007;33:1043–57.
11. Maniruzzaman M, et al. Drug-polymer intermolecular interactions in hot-melt extruded solid dispersions. Int J Pharm. 2013;443:199–208.
12. Ajjarapu S, et al. A rapid tool to optimize process variables for continuous manufacturing of metronidazole ointment using melt extrusion technique. AAPS PharmSciTech. 2020;21:273.
13. Shettar A, et al. Development and characterization of novel topical oil/PEG creams of voriconazole for the treatment of fungal infections. J Drug Deliv Sci Technol. 2021;66: 102928.
14. Hussain Shaik, Md Z, Shiva J, Venkateswarlu G, Suthakaran D, Ghouse S. Formulation and evaluation of ritonavir immediate release tablets by hot melt extrusion method. J Drug Deliv Ther. 2019;9:63–71.
15. Ma X, et al. Influence of carbamazepine dihydrate on the preparation of amorphous solid dispersions by hot melt extrusion. Pharm. 2020;12:379.
16. Sarabu S, et al. Preliminary investigation of peroxide levels of Plasdone™ copovidones on the purity of atorvastatin calcium amorphous solid dispersions: impact of plasticizers on hot melt extrusion processability. J Drug Deliv Sci Technol. 2022;70: 103190.
17. Almotairy A, et al. Investigation of hot melt extrusion process parameters on solubility and tabletability of atorvastatin calcium in presence of Neusilin® US2. J Drug Deliv Sci Technol. 2023;79: 104075.
18. Lin X, et al. Physical stability of amorphous solid dispersions: a physicochemical perspective with thermodynamic, kinetic and environmental aspects. Pharm Res. 2018;35:125.
19. Feng S, Bandari S, Repka MA. Investigation of poly(2-ethyl-2-oxazoline) as a novel extended release polymer for hot-melt extrusion paired with fused deposition modeling 3D printing. J Drug Deliv Sci Technol. 2022;74: 103558.
20. Zhang Z, Feng S, Almotairy A, Bandari S, Repka MA. Development of multifunctional drug delivery system via hot-melt extrusion paired with fused deposition modeling 3D printing techniques. Eur J Pharm Biopharm. 2023;183:102–11.
21. Hurley D, Potter CB, Walker GM, Higginbotham CL. Investigation of ethylene oxide-co-propylene oxide for dissolution enhancement of hot-melt extruded solid dispersions. J Pharm Sci. 2018;107:1372–82.
22. LaFountaine JS, et al. Thermal processing of PVP- and HPMC-based amorphous solid dispersions. AAPS PharmSciTech. 2016;17:120–32.
23. Thakkar R, et al. Novel on-demand 3-dimensional (3-D) printed tablets using fill density as an effective release-controlling tool. Polym. 2020;12:1872.
24. Maniruzzaman M, et al. Taste masking of paracetamol by hot-melt extrusion: an in vitro and in vivo evaluation. Eur J Pharm Biopharm Off J Arbeitsgemeinschaft Pharm Verfahrenstechnik EV. 2012;80:433–42.
25. Hunter LJ, Wood DM, Dargan PI. The patterns of toxicity and management of acute nonsteroidal anti-inflammatory

drug (NSAID) overdose. Open Access Emerg Med OAEM. 2011;3:39–48.

26. Passerini N, Albertini B, González-Rodríguez ML, Cavallari C, Rodriguez L. Preparation and characterisation of ibuprofen-poloxamer 188 granules obtained by melt granulation. Eur J Pharm Sci Off J Eur Fed Pharm Sci. 2002;15:71–8.

27. Seo A, Holm P, Kristensen HG, Schaefer T. The preparation of agglomerates containing solid dispersions of diazepam by melt agglomeration in a high shear mixer. Int J Pharm. 2003;259:161–71.

28. Serajuddin AT. Solid dispersion of poorly water-soluble drugs: early promises, subsequent problems, and recent breakthroughs. J Pharm Sci. 1999;88:1058–66.

29. Vilhelmsen T, Eliasen H, Schaefer T. Effect of a melt agglomeration process on agglomerates containing solid dispersions. Int J Pharm. 2005;303:132–42.

30. Alshahrani SM, et al. Stability-enhanced hot-melt extruded amorphous solid dispersions via combinations of Soluplus® and HPMCAS-HF. AAPS PharmSciTech. 2015;16:824–34.

31. Thakkar R, et al. A comparison between lab-scale and hot-melt-extruder-based anti-inflammatory ointment manufacturing. AAPS PharmSciTech. 2020;21:200.

32. Yu LX, et al. Understanding pharmaceutical quality by design. AAPS J. 2014;16:771–83.

33. Alzahrani A, et al. Design and optimization of ciprofloxacin hydrochloride biodegradable 3D printed ocular inserts: full factorial design and in-vitro and ex-vivo evaluations: Part II. Int J Pharm. 2023;631: 122533.

34. Weissman SA, Anderson NG. Design of experiments (DoE) and process optimization. A review of recent publications. Org Process Res Dev. 2015;19:1605–33.

35. Chavez P-F, et al. Optimization of a pharmaceutical tablet formulation based on a design space approach and using vibrational spectroscopy as PAT tool. Int J Pharm. 2015;486:13–20.

36. Goos P, Jones B, Syafitri U. I-Optimal design of mixture experiments. J Am Stat Assoc. 2016;111:899–911.

37. Politis N, S., Colombo, P., Colombo, G. & M Rekkas, D. Design of experiments (DoE) in pharmaceutical development. Drug Dev Ind Pharm. 2017;43:889–901.

38. Morott JT, et al. The effects of screw configuration and polymeric carriers on hot-melt extruded taste-masked formulations incorporated into orally disintegrating tablets. J Pharm Sci. 2015;104:124–34.

39. Dedroog S, Pas T, Vergauwen B, Huygens C, Van den Mooter G. Solid-state analysis of amorphous solid dispersions: why DSC and XRPD may not be regarded as stand-alone techniques. J Pharm Biomed Anal. 2020;178: 112937.

40. Bhide S, Panda A, Rangappa S, Shettar A, Repka MA, Prado R, Kundu S, Richardson N, Murthy SN. Evaluating the impact of fatty alcohols on permeation of clotrimazole from topical creams. Pharm Technol. 2020;44:24–31.

41. Karavas E, Georgarakis M, Docoslis A, Bikiaris D. Combining SEM, TEM, and micro-Raman techniques to differentiate between the amorphous molecular level dispersions and nanodispersions of a poorly water-soluble drug within a polymer matrix. Int J Pharm. 2007;340:76–83.

42. Kolimi P, et al. Development and validation of HPLC method for efinaconazole: application to human nail permeation studies. AAPS PharmSciTech. 2022;23:63.

43. Research, C. for D. E. and. Q1A(R2) stability testing of new drug substances and products. U.S. Food and Drug Administration https://www.fda.gov/regulatory-information/search-fda-guidance-documents/q1ar2-stability-testing-new-drug-substances-and-products (2020). Accessed 03/05/2018.

44. Noce L, Gwaza L, Mangas-Sanjuan V, Garcia-Arieta A. Comparison of free software platforms for the calculation of the 90% confidence interval of f2 similarity factor by bootstrap analysis. Eur J Pharm Sci Off J Eur Fed Pharm Sci. 2020;146: 105259.

45. Yuksel N, Kanik AE, Baykara T. Comparison of in vitro dissolution profiles by ANOVA-based, model-dependent and -independent methods. Int J Pharm. 2000;209:57–67.

46. Shankar VK, et al. Effect of lipid vehicles on solubility, stability, and topical permeation of delta-9-tetrahydrocannabinol. AAPS PharmSciTech. 2022;23:223.

47. Zhou W, Gilpin RK. Rapid ESI-MS method for examining the thermal decomposition of pharmaceuticals. J Pharm Sci. 2004;93:1545–56.

48. Abdul Mudalip SK, et al. Effects of solvents on polymorphism and shape of mefenamic acid crystals. MATEC Web Conf. 2018;150:02004.

49. Panchagnula R, Sundaramurthy P, Pillai O, Agrawal S, Raj YA. Solid-state characterization of mefenamic acid. J Pharm Sci. 2004;93:1019–29.

50. Real D, Orzan L, Leonardi D, Salomon CJ. Improving the dissolution of triclabendazole from stable crystalline solid dispersions formulated for oral delivery. AAPS PharmSciTech. 2019;21:16.

51. Ewing AV, Clarke GS, Kazarian SG. Stability of indomethacin with relevance to the release from amorphous solid dispersions studied with ATR-FTIR spectroscopic imaging. Eur J Pharm Sci Off J Eur Fed Pharm Sci. 2014;60:64–71.

52. Thenmozhi K, Yoo YJ. Enhanced solubility of piperine using hydrophilic carrier-based potent solid dispersion systems. Drug Dev Ind Pharm. 2017;43:1501–9.

53. Kuroiwa Y, Higashi K, Ueda K, Yamamoto K, Moribe K. Nanoscale and molecular-level understanding of wet-milled indomethacin/poloxamer 407 nanosuspension with TEM, suspended-state NMR, and Raman measurements. Int J Pharm. 2018;537:30–9.

54. Hillery AM, Florence AT. The effect of adsorbed poloxamer 188 and 407 surfactants on the intestinal uptake of 60-nm polystyrene particles after oral administration in the rat. Int J Pharm. 1996;132:123–30.

55. Wolfe JA, et al. Gastritis, duodenitis, and bleeding duodenal ulcer following mefenamic acid therapy. Arch Intern Med. 1976;136:923–5.

56. Gudis K, Sakamoto C. The role of cyclooxygenase in gastric mucosal protection. Dig Dis Sci. 2005;50(Suppl 1):S16-23.

57. Anderberg EK, Bisrat M, Nyström C. Physicochemical aspects of drug release. VII. The effect of surfactant concentration and drug particle size on solubility and dissolution rate of felodipine, a sparingly soluble drug. Int J Pharm. 1988;47:67–77.

58. Mehanna MM, Motawaa AM, Samaha MW. In sight into tadalafil - block copolymer binary solid dispersion: Mechanistic investigation of dissolution enhancement. Int J Pharm. 2010;402:78–88.